Ceramics International 51 (2025) 15402–15415

Contents lists available at ScienceDirect

Ceramics International

journal homepage: www.elsevier.com/locate/ceramint

Magnesium oxide coatings on thermoplastic polyurethane as a key approach to prevent catheter-associated infections

Tatiana Padrão [a,b,c,d,*], Fernando J. Monteiro [a,b,d,1], Susana R. Sousa [a,b,e,1], Juliana R. Dias [c,**,1]

[a] i3S – Instituto de Investigação e Inovação em Saúde, Universidade do Porto, Rua Alfredo Allen 208, 4200-135, Porto, Portugal
[b] INEB – Instituto de Engenharia Biomédica, Universidade do Porto, Rua Alfredo Allen 208, 4200-135, Porto, Portugal
[c] CDRSP – Centro para o Desenvolvimento Rápido e Sustentado de Produto, Instituto Politécnico de Leiria, Marinha Grande, 2430-028, Portugal
[d] FEUP – Faculdade de Engenharia, Universidade do Porto, Rua Dr. Roberto Frias, 4200-465, Porto, Portugal
[e] ISEP – Instituto Superior de Engenharia do Porto, Instituto Politécnico do Porto, Rua Dr. António Bernardino de Almeida 431, 4200-072, Porto, Portugal

ARTICLE INFO

Handling Editor: Dr P. Vincenzini

Keywords:
Antibacterial
Catheter
Infection
Magnesium oxide
Nanoparticles
Polyurethane

ABSTRACT

Central venous catheters (CVCs) are essential healthcare tools, but their use is often complicated by bacterial colonization on the catheter surface, leading to serious infections and life-threatening bloodstream complications. Current strategies, often reliant on antibiotics or antiseptics, are increasingly ineffective due to the rise of antimicrobial resistance. This study aimed to develop a novel antibacterial coating for CVCs by incorporating magnesium oxide (MgO) nanoparticles onto a thermoplastic polyurethane (TPU) film surface containing barium sulfate ($BaSO_4$). The antibacterial efficacy of these coatings was evaluated against *Staphylococcus epidermidis*, a major pathogen in catheter-associated infections. The results showed that MgO coatings significantly inhibited bacterial growth in a concentration-dependent manner, with 0.50 % and 1.0 % MgO concentrations achieving complete eradication of both planktonic and adherent bacteria. Importantly, the coatings exhibited excellent cytocompatibility with fibroblasts and showed no significant impact on hemolysis or blood clotting. The 0.50 % MgO coating was identified as the optimal formulation, offering the best balance of potent antibacterial activity, cytocompatibility and hemocompatibility. This approach preserves the valuable physical and chemical properties of the TPU material while providing effective antibacterial protection. The straightforward and cost-effective coating process holds significant promise for industrial scale production, paving the way for a new generation of safer and more effective CVCs.

1. Introduction

Hospital-acquired infections (HAIs) pose a significant public health concern, leading to increased patient morbidity, prolonged hospitalizations, and high healthcare costs [1]. In the United States of America (USA), approximately 1.7 million HAIs occur annually, being bacterial colonization and biofilm formation on medical devices responsible for over half of these cases [2–4]. Among several medical devices, central venous catheters (CVCs) are particularly prone to infections, contributing to serious complications such as bloodstream infections [1,5,6]. These infections affect up to 8 % of inserted catheters each year [7], resulting in hundreds of thousands of nosocomial bacteremia cases and significant economic costs ranging from $296 million to $2.3 billion annually in the USA [8,9]. CVC-related infections are associated with mortality rates between 12 % and 25 %, and are a leading cause of bacteremia and septicemia in hospitalized patients [10–12]. Over 5 million CVCs are implanted every year in the USA [13], primarily in critical care and chemotherapy settings, where patients are especially vulnerable to infection due to compromised immune systems [14,15]. Infections typically arise from bacteria colonization at the catheter hub or tubing, originating from patient's skin flora or external sources. *Staphylococcus epidermidis* is the predominant pathogen, responsible for 60–70 % of the episodes [16–18]. Occasionally, these infections can also arise from circulating bacteria contaminating the catheter lumen.

* Corresponding author. Alfredo Allen, 208, 4200 – 135, Porto, Portugal.
** Corresponding author. Rua de Portugal – Zona Industrial, 2430-028, Marinha Grande, Portugal.
E-mail addresses: tatiana.padrao@i3s.up.pt (T. Padrão), juliana.dias@ipleiria.pt (J.R. Dias).
[1] These authors contributed equally to this work.

https://doi.org/10.1016/j.ceramint.2025.01.376
Received 20 August 2024; Received in revised form 4 January 2025; Accepted 21 January 2025
Available online 22 January 2025

Microbial contamination, colonization and biofilm formation on catheter surfaces usually occur 24 h after insertion [19]. The current treatment typically includes catheter removal or replacement, along with antibiotic therapy, being inefficient in most cases of biofilm formation [20].

The strategies to prevent these infections, besides proper clinical handling, and manipulation practices, include prophylactic intravenous antibiotics and antiseptics [21]. Also, the commercial available antibacterial catheters often rely on antibiotics or silver-based coatings [8,22,23], but the rise of antibiotic-resistance bacteria and potential toxicity often make these products ineffective [24]. These limitations emphasized the urgent need for alternative materials capable of preventing microorganisms colonization and biofilm formation.

Inorganic nanoparticles, namely metal oxides, have received significant attention as antibacterial agents due to their high stability, safety, and long shelf-life, which are critical features for industrial and commercial applications [25]. Moreover, such nanoparticles show strong antimicrobial activity towards different microorganisms, positioning themselves as promising candidate alternatives to the use of traditional antibiotics [24,26,27]. Magnesium oxide (MgO) is a promising material low-cost and eco-friendly material, with excellent antimicrobial characteristics [28]. The exact mechanism underlying the antibacterial action of MgO and other metal oxide nanoparticles is still debated, being the formation of reactive oxygen species that cause oxidative stress, the most commonly reported mechanism in the literature [29]. MgO offers the advantage of being non-toxic as an antibacterial agent. Although metals and metal oxides such as silver, zinc oxide, copper oxide and titanium dioxide show antibacterial activity against various microorganisms, they associate heavy metal toxicity and potential for accumulation in the body poses significant risks. In contrast, MgO is a light metal-based material that can be metabolized in the body. It easily degrades into harmless Mg^{2+} and OH^- ions, which are naturally excreted through the renal system [29,30], making it a safe material, as recognized by the United States Food and Drug Administration (FDA) [31]. Additionally, Mg^{2+} ions participate in essential physiological processes [32,33] and have already been reported to have an anticoagulant effect [34], making MgO coatings particularly advantageous for blood contact applications like CVCs.

Thermoplastic polyurethane (TPU) is widely used in medical devices, including catheters, due to its resilience, flexibility, strength, and biocompatibility. Barium sulfate ($BaSO_4$) is often incorporated into polymers to enhance radiopacity for X-ray imaging, a valuable feature for CVCs placement [35]. To this date, from the best of our knowledge, no studies have explored MgO coatings on TPU or TPU/$BaSO_4$ films to develop antibacterial surfaces, highlighting a significant research gap.

This study aims to address this gap by incorporating MgO nanoparticles onto TPU/$BaSO_4$ film surfaces to develop effective antibacterial coatings for CVCs. Using dip coating, a process compatible with catheter manufacturing, MgO nanoparticles were applied at different concentrations. The antibacterial potential of these coatings was evaluated against *Staphylococcus epidermidis*, the common pathogen involved in catheter associated infections, targeting both planktonic and adherent bacteria. Additionally, the coatings were evaluated in terms of cytocompatibility and hemocompatibility to ensure their suitability for blood contact applications. This research represents a promising step toward safer and more effective materials for medical device applications.

2. Materials and methods

2.1. Production of MgO coatings on TPU films

2.1.1. Production of TPU films

Pellets of Tecothane TT-1095A medical grade thermoplastic polyurethane (TPU) were provided from Lubrizol Corporation (Ohio, USA). Pellets of Pellethane 2363-90A medical grade TPU +25 % $BaSO_4$ barium sulfate nanoparticles (TPU/$BaSO_4$) were purchased from Lubrizol Corporation (Ohio, USA) through Vygon Portugal. TPU and TPU/$BaSO_4$ films were prepared by solvent casting method [36], following several optimization steps. Briefly, once optimal conditions were established, TPU and TPU/$BaSO_4$ pellets, previously dried overnight at 60 °C, were dissolved at concentrations of 9.4 % (w/v) (weight of pellets per volume of solvent) and 12.5 % (w/v) for TPU and TPU/$BaSO_4$, respectively, in tetrahydrofuran (THF, Fisher Chemical UK) at room temperature (RT) for 18 h. Afterward, 20 mL of this solution was thoroughly cast into glass Petri dishes (Ø = 100 mm). Petri dishes were covered with perforated aluminum foil and left RT for 48 h for slow evaporation of THF. Then, they were placed in a vacuum oven overnight to ensure complete solvent evaporation and consequently avoid the formation of bubbles on the surface films. The resulting films were then extracted from the dishes and cut into squares measuring 1 x 1 cm^2.

2.1.2. Production of MgO coatings

TPU/$BaSO_4$ – MgO coated films were produced using MgO nanostructured powder as raw material. According to the manufacturer, the magnesium oxide (Alfa Aesar, Germany) used in this study was a nanopowder with an average particle size of 40–60 nm, purity >99 % (metal basis) and a bulk density of 3.58 g/cm^3 and further characterization was performed.

Coating formulations containing MgO were prepared by solvent mixing [37]. Initially, MgO dispersions were prepared in dimethylformamide (DMF, Carlo Erba Reagents, France) at different concentrations 0.05, 0.13, 0.50, 1.0 % (w/v) (weight of MgO per volume of solvent) under mechanical stirring at 200 rpm overnight. Subsequently, 1 h of ultrasonication was applied using a Digital Ultrasonic cleaner (200 W, 40 kHz, ArgoLab, DU-45, Italy) at RT. Then, TPU/$BaSO_4$ films were vertically immersed in the coating formulations for 20 s and dried for 14 h in a vacuum oven. TPU/$BaSO_4$ films coated with four different concentrations of MgO were successfully developed and named as 0.05, 0.13, 0.50 and 1.0 % MgO. TPU films were also used as a control for TPU/$BaSO_4$ films to confirm if $BaSO_4$ did not influence its properties. Materials sterilization was performed under UV light for 15 min on each side, before biological tests characterization.

2.2. Physico-chemical characterization

The coating of the MgO on TPU/$BaSO_4$ film surface was evaluated by Fourier Transform Infrared Spectroscopy with Attenuated Total Reflectance (FTIR-ATR), MgO dispersion in the polymer was followed by Scanning electron microscopy (SEM), surface topography was also characterized by transmission electron microscopy (TEM), wettability was evaluated by captive bubble contact angle measurements and the surface charge was followed by zeta potential measurements.

2.2.1. Scanning electron microscopy

SEM and energy-dispersive X-ray spectroscopy (EDS) were used to observe the morphology of the TPU and TPU/$BaSO_4$ films' surface and cross-section and to carry out a semiquantitative analysis of their elemental chemical composition. The analysis was performed using a high-resolution scanning electron microscope FEI Quanta 400 FEG/ESEM/EDAX Genesis X4M, with X-ray microanalysis and electron backscattered diffraction analysis at an accelerating voltage of 15 kV. X-ray mapping and backscattered electron images were additionally acquired to enhance the visualization of MgO particle distribution across the surface film. After being frozen in liquid nitrogen, the films were fractured transversely. They were placed on conductive carbon tape fixed on aluminum sample holders and both the top surface and the fractured cross-section surface were analyzed. Prior to analysis, the samples were sputtered with Au/Pd alloy conductive thin film using a SPI Module sputter coater for 80 s under 15 mA current to provide electrical conductivity. The depth at which the MgO particles were found was measured in the cross-section images using Image J software

(Fiji, version J1.46r., NIH, Bethesda, MD, USA).

2.2.2. Transmission electron microscopy

For the analysis of the TPU/$BaSO_4$ – MgO coated films, the samples were embedded in Embed-812 resin (#14120; Electron Microscopy sciences). Ultra-thin sections (50 nm thickness) were cut on an RMC Ultramicrotome (PowerTome, USA) using Diatome diamond knifes, mounted on mesh copper grids (Electron Microscopy Sciences, Hatfield, PA, USA). For TEM analysis of MgO nanopowder, a small amount of MgO particles were placed on 200 mesh copper TEM grid. All samples were analyzed on a JEOL JEM 1400 TEM (JEOL, Tokyo, Japan) and images were digitally recorded using a CCD digital camera Orius 1100W (Tokyo, Japan).

2.2.3. Fourier transformed infrared spectroscopy

Chemical characterization of TPU and TPU/$BaSO_4$ films and TPU/$BaSO_4$ - MgO coated films was performed using Fourier transformed infrared spectroscopy (FTIR) with attenuated total reflection (ATR). ATR-FTIR spectra were acquired (Universal ATR module coupled to a PerkinElmer Frontier) with an average of 32 consecutive interferograms at 4 cm^{-1} resolution, between 4000 and 400 cm^{-1} and using a MIRTGS (mid infrared Telurium Glycine sulfate) detector. Spectra were fitted using the Spectrum (version 10.5.2.636) software. The chemical composition of MgO nanopowder was also evaluated using a Slide Holder accessory coupled to FTIR spectrometer and the samples were reduced to power and analyzed as KBr pellets.

2.2.4. Contact angle measurements

Wettability studies of TPU and TPU/$BaSO_4$ films and TPU/$BaSO_4$ - MgO coated films were performed using a video-based optical contact angle measurement device OCA 15 plus, provided with an electronic syringe unit (Dataphysics Instruments GmbH, Germany). Type II ddH_2O was used and measurements were carried out at RT. Static contact angles were measured at RT by the sessile drop method on droplets of 4 μL for water deposited on the surface. At least five drops were made per sample type in three different samples. Contact angles were calculated by SCA20 software (Dataphysics, version 2.0), fitting the drop profiles to the Young-Laplace equation. Results are reported as mean value ± standard deviation (SD).

2.2.5. Zeta potential

The Zeta potential of films was assessed to determine whether the incorporation of MgO into the material would affect its surface charge. With that purpose, streaming potential measurements were obtained using a commercial electrokinetic analyzer (EKA) (Anton Paar GmbH, Austria) using a special rectangular cell for small flat samples with a variable channel height.

One sample (2 × 1 cm) was glued on each poly-methyl methacrylate (PMMA) block and mounted in parallel on each side of the cell, creating a rectangular (2 × 1 cm^2) slit channel between the sample surfaces. The height of the slit channel was maintained constant for all the measurements using a micrometer screw, adjusting it after checking the flow in each direction. The streaming potential was measured using Ag/AgCl electrodes installed at both ends of the streaming channel. The electrolyte used was 1 mM KCl with pH between 5.7 and 7.4. Experiments were performed at RT. The conductivity of the electrolyte solution was measured throughout the assay. The streaming potential was measured by applying an electrolyte flow in alternating directions, with pressure ramps ranging from 0 to 400 mbar. For each surface, twelve pressure ramps were conducted, six in each flow direction, to cope with the asymmetric potential fluctuations.

2.3. Degradation studies

The primary goal of performing degradation studies was to check the stability and durability of the coatings on TPU/$BaSO_4$ – MgO coated films. The degradation studies were developed in accordance with ISO 10993:2001 - Biological evaluation of medical devices—Part 14: Identification and quantification of degradation products from ceramics [38], using Tris-HCl buffered solution (pH = 7.4). The films, cut into 1 × 1 cm^2 squares, were immersed in buffer solution at 37 °C under stirring at 120 rpm in an orbital shaker (KS 4000 IC, IKA®). After each immersion during 1, 3, 7, 14 and 28 days, the solution was withdrawn, and the films were exposed to vacuum oven drying until being completely desiccated. The weight loss for each material was calculated using the formula:

$$Weight\ loss = \frac{W_0 - W_t}{W_0} \times 100\ \% \quad \text{(Eq. 2)}$$

Where W_0 and W_t represent the initial weight and weight after a specific immersion time, respectively. The resultant solution at each immersion time was preserved for measurements and quantification of Magnesium using Inductively Coupled-Plasma Atomic Emission Spectroscopy (ICP-AES). The analysis was carried out on a Horiba Jobin Yvon ULTIMA sequential ICP, with the Horiba Jobin Yvon ICP Analyst 5.4 software. A monochromator equipped with a Czerny Turner spectrometer was employed, and Argon was used as the gas. This test was performed with three replicates per sample. The total amount of Mg present in each film was also determined by ICP-AES after the samples had been digested. This test was performed with five replicates per sample. The results were expressed as mean ± SD values of measurements.

2.4. Antibacterial assays

2.4.1. Bacterial strains, media and culture conditions

Staphylococcus epidermidis (ATCC 35984) were obtained from the American Type Culture Collection (Manassas VA, USA). Bacteria were maintained at - 80 °C in a solution containing 70 % tryptic soy broth (TSB) (Merck, Germany) and 30 % diluted glycerol. Bacteria were inoculated from the frozen stock in tryptic soy agar (TSA) (Merck, Germany) plates overnight at 37 °C. Two to three colonies were collected, incubated into 10 mL of TSB overnight at 37 °C, under stirring at 150 rpm.

2.4.2. Determination of minimum inhibitory concentration and minimum bactericidal concentration of MgO nanopowder

To access the antibacterial activity of MgO, minimum inhibitory concentration (MIC) and minimum bactericidal concentration (MBC) values were determined, using the broth microdilution method according to CLSI M07 (Clinical and Laboratory Standards Institute, M07: Methods for Dilution Antimicrobial Susceptibility Tests for Bacteria that Grow Aerobically) [39]. Briefly, the microbiological media and a range of MgO concentrations were prepared, the bacteria were cultured, and the broth microdilution assay was initiated. After bacteria incubation, the bacterial growth was quantified by counting the number of colony-forming units (CFUs) to determine the number of cultivable cells.

To prepare the MgO suspensions, the MgO was added to 0.9 % sodium chloride (NaCl) (Sigma-Aldrich, USA) to obtain concentrations between 0.5 mg/mL and 8 mg/mL. The MgO concentrations were selected because this range includes various concentrations that have been reported in the literature to present antimicrobial activities [29,40,41]. Specifically, an initial solution of 10 mg/mL was prepared and subsequently diluted to obtain six different concentrations of MgO (0.5, 1, 2, 4, 6 and 8 mg/mL).

1 mL of overnight cultures, containing the bacterial strain on stationary phase, as previously described, was inoculated into 10 mL of fresh TSB. Then, this culture was incubated for 3 h at 37 °C to obtain the bacterial suspension on exponential phase (ca., 10^8 CFU/mL). Then, the suspension was diluted 1/100 in TSB to obtain the desired concentration of 10^6 CFU/mL. Samples without MgO were used as a positive control (Bacteria with NaCl). A negative control was also used by incubating

each MgO concentration in TSB without adding any bacterial cells. The plates were incubated for 24 h at 37 °C in an orbital shaker (150 rpm). Five replicates were used for experimental and control samples.

For CFUs quantification, the standard plate count was used, which is a procedure for estimating the number of CFUs, corresponding to the cultivable/viable bacteria. With this purpose, the bacterial suspension was serially diluted in 0.9 % NaCl. Afterward, 10 μL of the serial dilutions were spread onto the TSA plates. The plates were incubated for 18 h at 37 °C. Subsequently, the number of colonies was counted. Results were expressed as the decimal logarithm of the CFU per milliliter of suspension as follows:

$$CFU \Big/ mL = \frac{number\ of\ colonies\ counted}{dilution \times volume\ of\ sample\ plated, mL} \quad \text{(Eq. 1)}$$

2.4.3. Antibacterial activity of coatings

The antibacterial activity of the surfaces was evaluated according to ISO 22196:2007 (Plastics – Measurement of antibacterial activity on plastics surfaces and other non-porous surfaces) [42]. TPU and TPU/-$BaSO_4$ films and TPU/$BaSO_4$ – MgO coated films were cut into disks Ø = 10.5 mm, and placed in 24-well plates. The bacterial suspension was adjusted to 6 × 10^5 CFU/mL in fresh TSB medium using a UV–Vis molecular absorption spectrophotometry (SPECTROstarNano, BMG LABTECH, Ortenberg, Germany). A 14 μL drop of the bacterial suspension was applied on top of each sample and covered with a sterilized polypropylene coverslip (Ø = 8.5 mm) to ensure contact between bacteria and the sample surface. The samples were then incubated for 24 h at 37 °C in static and moisturized conditions, with the remaining empty wells were filled with distilled water (dH_2O) and the plates placed inside a container with moistened paper to prevent water evaporation. Control samples of TPU and TPU/$BaSO_4$ were used to measure viable cells after inoculation determining the bacterial recovery rate from the test specimens. Negative controls were obtained by incubating materials with only TSB medium, without bacteria, as contamination controls. After 24 h incubation, samples were rinsed with 350 μL of fresh TSB to detach the polypropylene coverslip and loosely adherent bacteria. The supernatant was collected to evaluate planktonic bacteria, and the materials were then used to assess sessile bacteria.

2.4.3.1. Planktonic bacteria. For planktonic bacteria quantification, after 24 h incubation with the materials, the supernatant was removed and serially diluted in 0.9 % NaCl (Sigma-Aldrich, USA). Then, 10 μL of each serial dilutions were inoculated in TSA plates, incubated at 37 °C for 18 h and the colony-forming units (CFU) counted for cell viability evaluation. Results were expressed as the decimal logarithm of the CFU per milliliter of suspension. All tests were performed in triplicate, with five replicates per sample.

2.4.3.2. Sessile bacteria. For sessile bacteria quantification, the materials were removed to new 24-well plate and carefully rinsed three times with 0.9 % NaCl to remove non-adherent or loosely adherent bacteria. Then, the materials were sonicated for 10 min in an ultrasonic bath (Argo lab, DU-45, Italy) to release the adherent bacteria. Finally, the sonicated solutions were used to obtain the serial dilutions, that were placed in TSA plates and incubated at 37 °C for 18 h. Colony counting was carried out, and the number of adherent bacteria was expressed in $\log_{10}$(CFU/mL). All experiments were performed in triplicate, with five replicates per sample.

2.4.3.3. S. epidermidis adhesion and morphology. SEM observation was used to evaluate the morphology of adherent *S. epidermidis* to films surfaces and changes in bacteria morphology. After incubation with bacterial suspension, the materials with adhered *S. epidermidis* were rinsed with PBS and fixed with 3 % (v/v) glutaraldehyde (Merck) in 0.14 M sodium cacodylate buffer (Merck) for 30 min at RT. Then, the samples were dehydrated in a gradient ethanol solutions series (50, 60, 70, 80, 90, 100 %) for 15 min each. The adherent *S. epidermidis* remaining on the film's surfaces were dried overnight at RT and prepared for SEM visualization as previously described.

2.5. In vitro cytotoxicity tests

The cytocompatibility of TPU, TPU/$BaSO_4$ films and TPU/$BaSO_4$ – MgO coated films were evaluated by direct contact and indirect contact assays toward L929 fibroblasts, according to the ISO 10993:2009 – Biological evaluation of medical devices – Part 5: Test for *in vitro* cytotoxicity [43].

2.5.1. Cell line and culture conditions

L929 (murine CCL-1, ATCC) fibroblasts derived from connective mouse tissue cell line were grown in alpha minimum essential medium (α- MEM) (Gibco, USA), supplemented with 1 % (v/v) penicillin-streptomycin (Pen/Strep) (Biowest, France) and 10 % (v/v) fetal bovine serum (FBS) (Gibco, USA). After confluence, the cells were detached with trypsin and seeded into 96-well plates at a density of 1 × 10^5 cells/mL and maintained at 37 °C in a humidified atmosphere containing 5 % CO_2 for 24 h (indirect assay). In parallel, cells in 1 × 10^5 cells/mL density were seeded in 24-well plates and maintained at 37 °C in a humidified atmosphere containing 5 % CO_2 for 24 h (direct assay).

For the direct contact assay, once the cells reached subconfluency, the culture medium was discarded, and fresh medium was added to each well. Afterward, the films (1 × 1 cm^2) were carefully placed on the cell layer. The cells were then incubated for 24 h under the above-mentioned conditions.

For the indirect contact assay, extracts were prepared according to ISO 10993:2009 – Biological evaluation of medical devices – Part 12: Sample preparation and reference materials. Briefly, films were incubated in cell culture medium in a mass/volume ratio of 6 cm^2/mL for 24h at 37 °C in a humidified atmosphere containing 5 % CO_2.

After cell seeding and incubation for 24 h, the culture medium was replaced by 100 μL extracts and re-incubated for another 24 h. The cell culture medium was used for negative control and for positive control of cytotoxic 1 % (v/v) Triton X-100 (Sigma Aldrich, USA).

2.5.2. Resazurin assay

The cells metabolic activity was assessed by the resazurin assay. Briefly, metabolically active cells can reduce the blue compound resazurin into resorufin, turning into pink-purple appearance that can be detected by spectroscopy. With this purpose, 10 % (v/v) resazurin was added to the cells and incubated for 3 h at 37 °C in a humified atmosphere of 5 % CO_2. Afterward, 100 μL were transferred to a black 96-well plate and fluorescence was measured at excitation and emission wavelengths of 530 and 590 nm, respectively, using a SynergyMx fluorimeter (BioTek, USA). Results represent the average of three independent experiments. For each experiment five replicates were used per group and data were normalized with respect to the negative control.

2.5.3. Live/dead cell staining

Cell viability was assessed using Live/dead cell staining, which simultaneously quantifies live and dead cells. Calcein-AM enters live cells and emits green fluorescence, propidium iodide (PI) enters cells with damaged membranes and binds to nucleic acids producing a bright red fluorescence. Cells were incubated with samples for 24 h, using 1 % Triton X-100 as a positive control and supplemented cell culture medium as negative control. Afterward, samples and controls were removed, and cells were washed with PBS. Additionally, 50 μL of Calcein AM (≥90 %, Sigma-Aldrich, USA) at a concentration of 1 μL/mL of α-MEM (Gibco, USA) and 50 μL PI solution (BD Biosciences, San Diego, USA) were added to each well and then the cells were incubated in the dark for 30 min at 37 °C. Once stained, the medium was removed, PBS was added to each well and cells were observed under an AxioObserver Z1 inverted fluorescence microscope (Zeiss, Germany) at an objective

magnification of 10× under a multidimensional acquisition mode 488 nm (calcein-AM) and 568 nm (PI) channels. The images were processed with Zen Blue software from Zeiss.

2.6. Hemocompatibility of coatings

The hemocompatibility of films were assessed toward hemolytic and thrombogenic potential. Human buffy coats and plasma were obtained from Immuno-hemotherapy Service Hospital São João, Porto, Portugal according to ethical approval established with INEB/i3S.

2.6.1. Hemolysis assay

To determine the hemolytic potential of the film surfaces, samples (1 × 1 cm^2) previously sterilized were incubated with red blood cells (RBCs). RBCs were isolated from human buffy coats through differential centrifugation at 400 G for 30 min [44]. After centrifugation, the upper layer, which containing plasma and mononuclear cells, was discarded, and the lower layer, containing RBCs, was washed three times with PBS. The isolated RBCs were then diluted to a cell density of 2.0 × 10^8 cells/mL, and 500 μL were added to the materials and incubated for 3 h at 37 °C in 24-well suspension plates. Plates were centrifuged at 4000 rpm for 15 min, after which 100 μL of the supernatant was transferred to 96-well plates. The absorbance was then measured at 380, 415 and 450 nm using a microplate reader spectrophotometer (Synergy MX, BioTek, USA). The amount of released hemoglobin (Hb) was determined following the equation (Eq. (3)):

$$Hb\ (mg.dL^{-1}) = \frac{(2 \times A415 - (A380 + A450)) \times 1000}{E} \quad \text{(Eq. 3)}$$

with A415, A380, and A450 representing the absorbance values of the samples at 415, 380, and 450 nm, respectively. E corresponds to the molar absorptivity of oxyhemoglobin at 415 nm [45]. The hemolytic potential was calculated according to the equation (Eq. (4)):

$$Hemolysis\ (\%) = \frac{Hb\ sample}{Hb\ total} \times 100 \quad \text{(Eq. 4)}$$

where Hb total represents the total amount of hemoglobin released (100 % hemolysis) under triton 1 % conditions. These tests were performed in triplicate, with five replicates per sample.

2.6.2. In vitro thrombogenicity assay

The anti-thrombogenic properties of TPU and TPU/$BaSO_4$ films and TPU/$BaSO_4$ - MgO coated films were evaluated using recalcified plasma clotting time method. To prepare the recalcified plasma, a 1 M stock solution of $CaCl_2$ was prepared and mixed with human plasma (citrate anticoagulated and thawed at 37 °C) to achieve a final calcium concentration of 20 mM. The recalcified plasma was then thoroughly vortexed and 500 μL of plasma were immediately added to each well plate of the 24-well suspension plate containing the samples (1 × 1 cm^2). Glass was used as a positive control for thrombogenicity, while polystyrene (PS) was the negative control (PS sample means the well plate only). The reference glass was rinsed in nitric acid for 8 h, washed three times with dH_2O, and dried at 37 °C overnight. Subsequently, the plates were incubated in an orbital shaker (KS 4000 IC, IKA®) at 37 °C and 150 rpm. The clotting time was determined as the time for the plasma to undergo gelation, indicated by the cessation of movement in response to the rotation and shaking. All tests were performed in triplicate, with three replicates per sample.

2.7. Statistical analysis

Statistical analysis was carried out using GraphPad Prism 8 software (GraphPad, USA). The data are presented as mean ± standard deviation (SD). The normality test of the population distribution was evaluated, and either parametric or non-parametric tests were employed accordingly, for normal or non-normal distributed data, respectively. For normally distributed data, one-way ANOVA followed by Tukey's multiple comparison test was used. For non-normally distributed data, the Kruskal-Wallis test was applied. Statistical significance was considered when $p < 0.05$ and represented with * for $p < 0.05$, ** for $p < 0.01$, *** for $p < 0.001$ and **** for $p < 0.0001$.

3. Results and discussion

3.1. Physico-chemical characterization of TPU/$BaSO_4$ – MgO coated films

3.1.1. Morphologic and topographic characterization

TPU and TPU/$BaSO_4$ films with smooth flat surfaces were successfully produced (macroscopic view Fig. S1 in Supplementary Material). A homogeneous TPU surface, devoid of pores, wrinkles, or irregularities is visible, as later confirmed by SEM images. Similarly to TPU films, TPU/$BaSO_4$ films also exhibit a smooth, bright surface with a white appearance due to the presence of uniformly distributed $BaSO_4$ nanoparticles, as further confirmed by SEM. The $BaSO_4$ nanoparticles provide radiopacity to the TPU, a requirement for applications such as CVCs, as they need to be contrasted via X-rays after insertion into the patient to confirm their insertion position. For this reason, MgO coatings were applied onto the TPU/$BaSO_4$ films, using the dip coating technique (macroscopic view Fig. S1 in Supplementary Material). MgO concentrations varied between 0.05 and 1.0 % (w/v) to confirm if there was a direct relationship between MgO concentration and surface exposure.

SEM images provided direct observation of the surface morphology of developed films. Particularly, the back-scattered electrons images highlight the presence of MgO particles on the TPU surface (white arrows) (Fig. 1). Their quantity increased with MgO concentration. The MgO nanoparticles tended to agglomerate, forming larger secondary particles that were uniformly dispersed within the TPU matrix. The tendency for particle aggregation is attributed to the large specific surface area characteristic of MgO nanoparticles. This agglomeration is also observed in the particles themselves prior to their inclusion in the coating, as evidenced by the TEM images (Fig. S2 A, Supplementary Material). A preliminary characterization using TEM was carried out to analyze the structure and morphology of the MgO nanostructured powder and it was possible to observe the presence of agglomerated nanoparticles. Under higher magnifications, it was possible to observe the spherical morphology of the MgO particles and their nanometric size (Fig. S2 D, Supplementary Material). Most of the measured particles had sizes between 40 and 60 nm, which agrees with the information provided by the manufacturer. TEM analyses of the TPU and TPU/$BaSO_4$ - MgO coated films were also carried-out, and the resulting images are depicted in Fig. 1C, with MgO particles highlighted with white arrows.

EDS global spectra were obtained to help to detect the MgO content, all analyses were obtained from the films' surfaces. From a qualitative perspective, it may be seen that higher magnesium peaks corresponded to the samples with higher MgO concentrations. On the other hand, carbon and oxygen peaks remained identical for all the samples, while the presence of barium and sulfur peaks was observed in all TPU/$BaSO_4$, with and without coating, as expected.

Besides being visible on the surface, the images of films' cross-sections revealed that MgO particles were able to penetrate up to 1–2 μm underneath the surface, regardless of their concentration, with particles visibly present within TPU/$BaSO_4$ matrix (white arrows). Furthermore, higher MgO concentrations corresponded to increased density in depth.

Semi-quantitative elemental EDS analysis of developed coated film surfaces and cross-sections was also performed on distinct regions for TPU and MgO and $BaSO_4$ nanoparticles. Considering TPU/$BaSO_4$ film coated with 0.50 % (w/v) MgO, the presence of MgO was clearly visible at the surface (Fig. 2 A), when there was no polymer overlaying and in such cases the carbon (C) peak in the EDS was short, indicating the

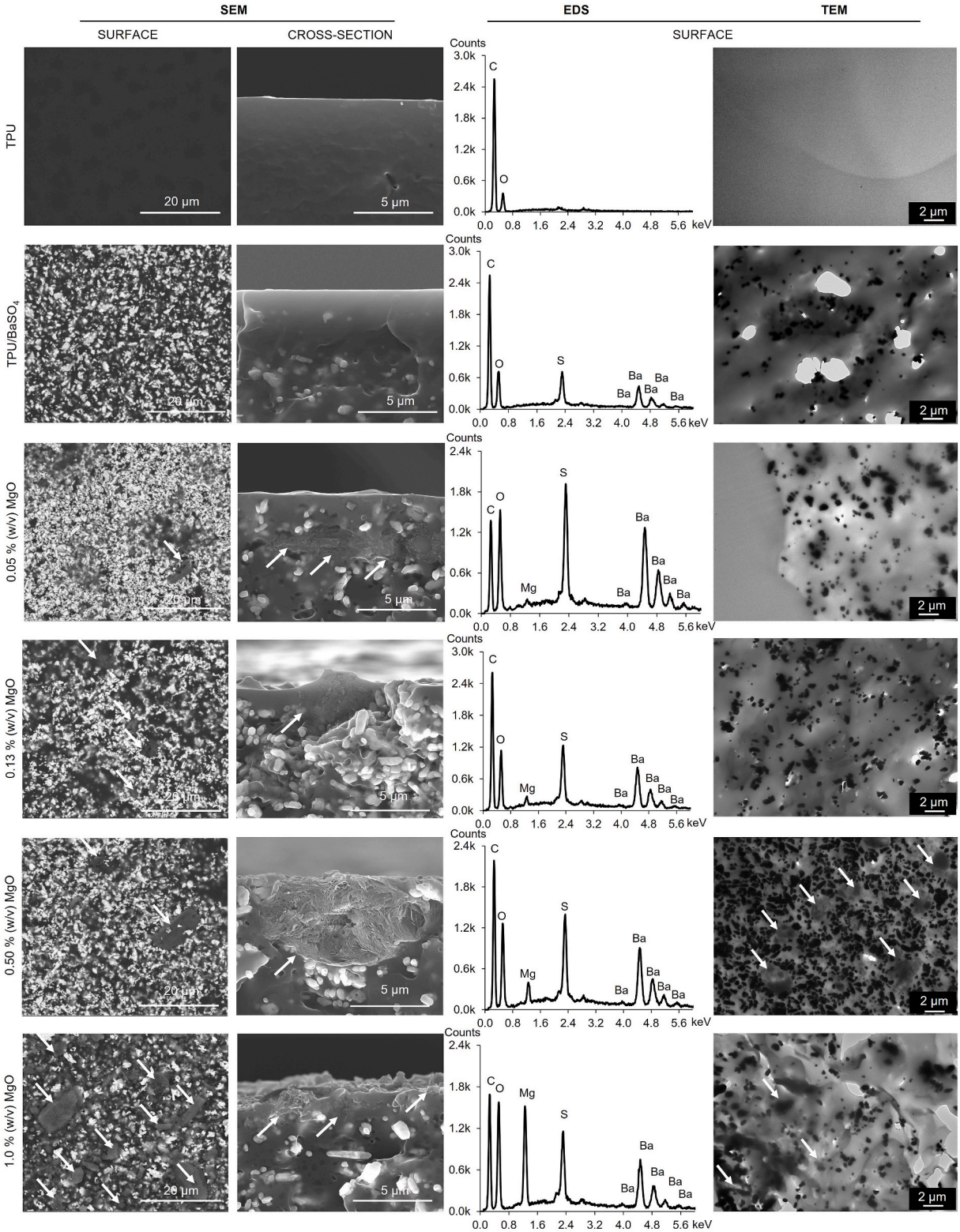

Fig. 1. – SEM Morphological and topographic characterization of TPU and TPU/$BaSO_4$ films coated with different concentrations of MgO on surface at a magnification of 5000x (scale bar = 20 µm, HV 15 kV, backscattered electrons (BSE) mode), showing the uniform distribution of MgO on the surface, with white arrows indicating MgO regions and cross-section view at a magnification of 20000x (scale bar = 5 µm, HV 15 kV, secondary electrons (SE) mode). EDS analysis confirming the presence of MgO nanoparticles within the coatings and TEM images (scale bar = 2 µm) providing further details on the dispersion and size of MgO.

absence of polymer on top of the sample (Z1). The EDS performed on the region with polymer at the top surface (Z2) presented the expected elements (C, O) with more intense peaks, while for the region with $BaSO_4$ nanoparticles (Z3) the presence of more intense peaks of Ba and S was detected. EDS analysis performed on the cross-section of the TPU/$BaSO_4$ film coated with 1.0 % (w/v) MgO (Fig. 2 B) confirmed the presence of MgO within the TPU/$BaSO_4$ matrix, corroborating what was previously observed by SEM, as evidenced in the marked regions Z2 and Z1, where,

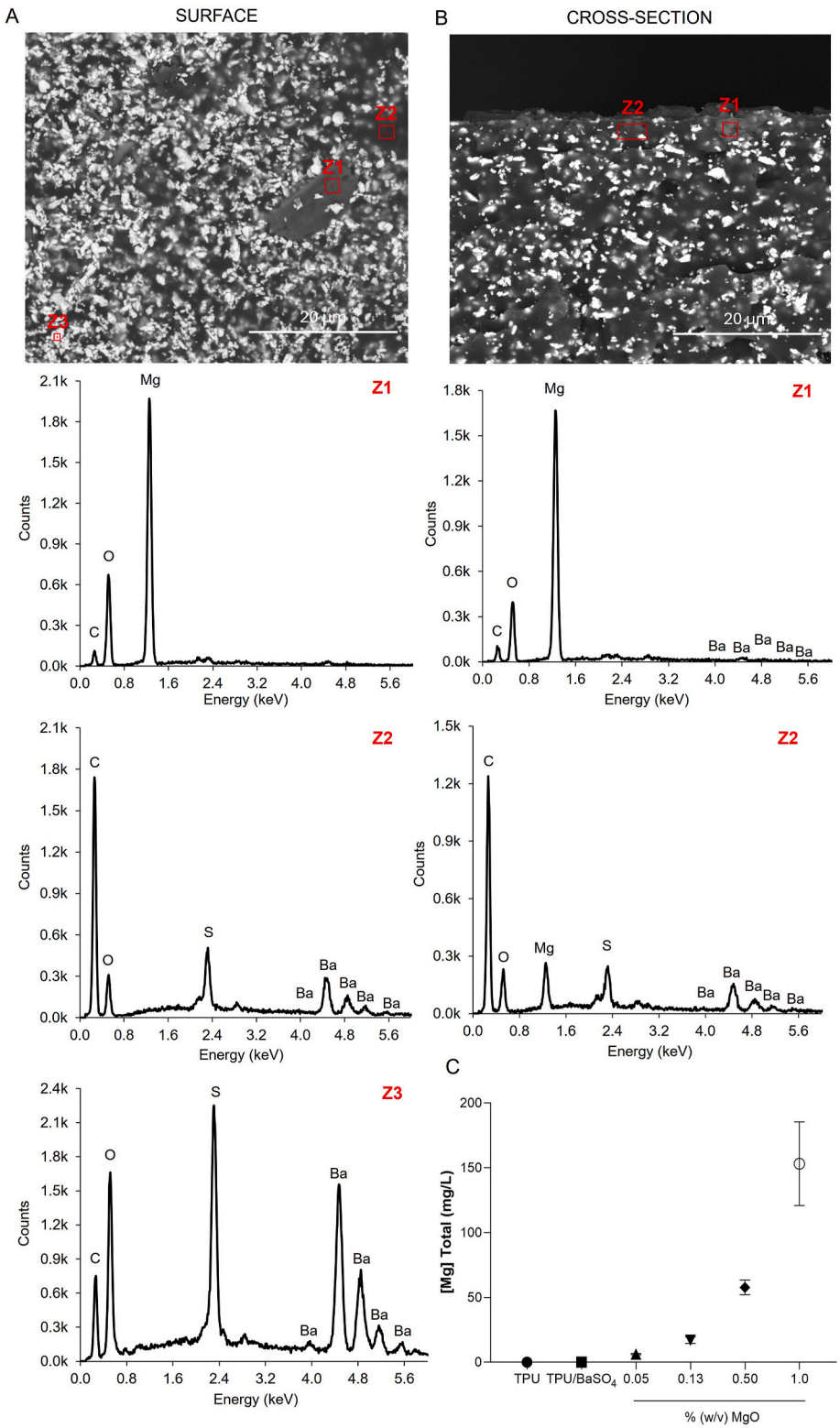

Fig. 2. –Semi-quantitative elemental EDS analysis of TPU/$BaSO_4$ with 0.50 % (w/v) MgO films. (A) EDS analysis of the surface of TPU/$BaSO_4$ with 0.50 % (w/v) MgO film, showing the distribution of elements across the coating surface. (B) EDS analysis of the cross-section of TPU/$BaSO_4$ with 1.0 % (w/v) MgO film, highlighting different regions: MgO region (Z1), polymer region (Z2) and $BaSO_4$ region (Z3) SEM images at a magnification of 5000x (scale bar = 20 µm, HV 15 kV, BSE mode). C) Total magnesium (Mg) concentration in the coated films as determined by inductively coupled plasma analysis. The results are expressed as mean ± SD (n = 5), showing the total concentration of Mg in the films at different coating conditions.

in region Z1, the exposed MgO particle is visible and confirmed by the high Mg peak and low C peak, as well as less prominent regions indicating the presence of MgO due to the polymer layer covering it, with more intense C peaks.

These results suggest that the dip coating technique with the dispersion in an organic solvent allowed for a partial solubilization of the upper layer of the polymer leading the surface to be permeabilized and the MgO to penetrate slightly deeper, in addition to its exposure at the surface.

Quantitative analysis of Mg total concentrations in the films using ICP analysis is represented in Fig. 2C. The results revealed uniformly increasing concentrations of Mg (standing for MgO particles) with increasing initial concentration in the coating formulations with 6.25 ± 0.45 mg/L for samples coated with 0.05 % MgO, 17.0 ± 2.2 mg/L for 0.13 % MgO, 57.7 ± 5.1 mg/L for samples coated with 0.50 % MgO, and 153 ± 29 mg/L for 1.0 % MgO.

X-ray mapping images were acquired to enhance the visualization of the MgO distribution on the polymer surface (Fig. 3). Since the presence of $BaSO_4$ nanoparticles in the TPU matrix may difficult/camouflage the clear observation of MgO, X-ray mapping was employed to enhance distinction and improve the MgO distribution observation. These images revealed that Mg were distributed in a relatively uniform manner across the surface, in larger amounts as the concentration of MgO rose (the signal strength is proportional to the content of MgO particles and there are also particle agglomeration areas that display bright signals), which is crucial to ensure effective interaction and inhibition of bacterial activity. Additionally, the distribution of Ba within the polymer was also obtained and is marked in the yellow signals.

3.1.2. Surface functional groups

Fig. 4 presents the FTIR spectra of TPU, TPU/$BaSO_4$ films, and TPU/$BaSO_4$ films coated with different MgO concentrations. For all materials, typical bands of TPU were observed, specifically the bands at 1527 cm^{-1} from N-H and C-H, at 1699 cm^{-1} from C = O related to urethane groups, at 1413 cm^{-1} and 1596 cm^{-1} associated to the benzene ring. The additional bands at 1225, 1182 and 984 cm^{-1} from symmetric stretching vibrations of the SO_4^{2-} group and the bands at 636 cm^{-1} and 610 cm^{-1} associated to the bending vibrations of SO_4^{2-}, characteristic of $BaSO_4$ [46,47] were also observed for all TPU/$BaSO_4$ films. Considering the films coated with MgO particles, the bands at 600 and 410 cm^{-1} correspond to the Mg-O vibrational mode, which became more evident as the MgO concentration increased. Also, it is possible to observe the appearance of a new band for the highest MgO concentrations, at 3700 cm^{-1} related with the stretching vibrations of OH^- groups, that were adsorbed on the MgO surface [48]. FTIR spectra of MgO particles were also carried out and the MgO characteristic bands are represented on Fig. S2 C (Supplementary Material).

3.1.3. Wettability

In terms of surface wettability, all materials presented similar water contact angles, approximately 90°, indicating a moderately hydrophobic surface (Fig. 5). Other authors, who also produced TPU films by solvent casting technique, reported similar water contact angles [49]. However, the introduction of MgO coating revealed significant differences compared to TPUs. The incorporation of 0.05, 0.13, 0.50 and 1.0 % (w/v) MgO led to a significant increase in TPU hydrophobicity, which an increase in contact angle ranging from 5° to 10°. For instance, the addition of 1.0 % MgO to the TPU/$BaSO_4$ surface film slightly increased the contact angle to 103.8° ± 13.9°. Souza et al. also observed an increase in the water contact angle with the addition of MgO to a polymeric matrix [35].

3.1.4. Surface charge

Table 1 shows the average zeta potential of TPU, TPU/$BaSO_4$ films and TPU/$BaSO_4$- MgO coated films. All materials presented negative charge. The presence of MgO might be the main factor contributing to the alteration in zeta potential, with coatings containing higher MgO concentrations showing more negative charges. The charge properties of both bacteria and material surfaces play a crucial role in bacterial adhesion. Bacteria typically have a negative charge at biological pH [50], which may result in electrostatic repulsion when in contact with material surfaces with similar negative charges, potentially inhibiting adhesion.

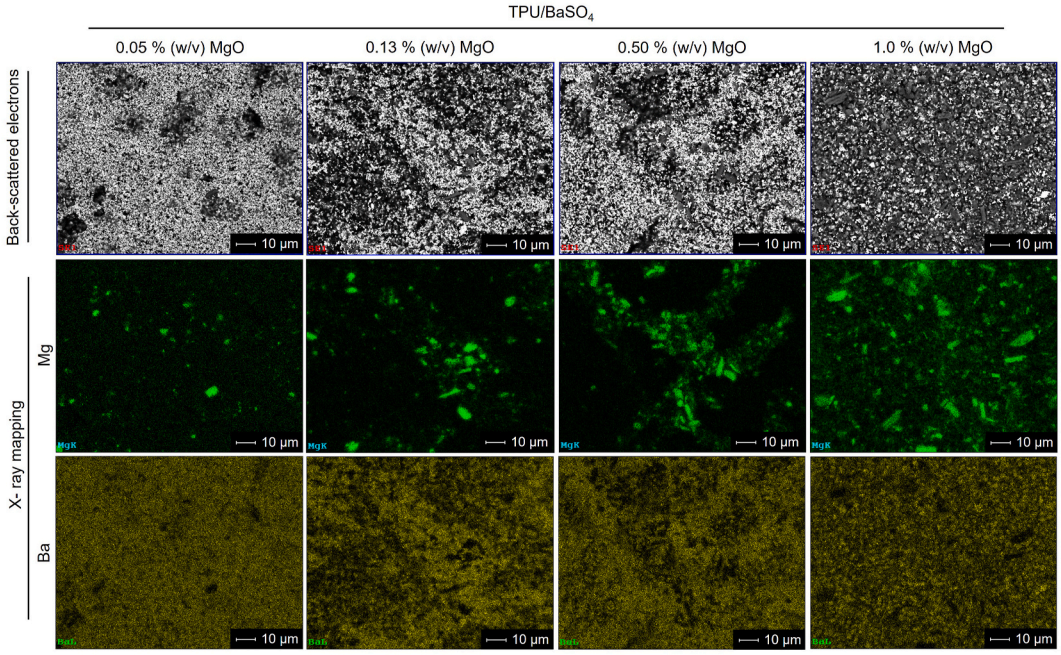

Fig. 3. Backscattered electrons (BSE) images and corresponding X-ray mapping of TPU/$BaSO_4$ films coated with different percentages of MgO. The X-ray maps show the distribution of MgO particles across the film surfaces (highlighted in green). BSE images present the same regions, with MgO particles in dark grey and $BaSO_4$ particles in light grey. Magnification for all images: 1000× (scale bar = 10 µm, HV 15 kV). (For interpretation of the references to colour in this figure legend, the reader is referred to the Web version of this article.)

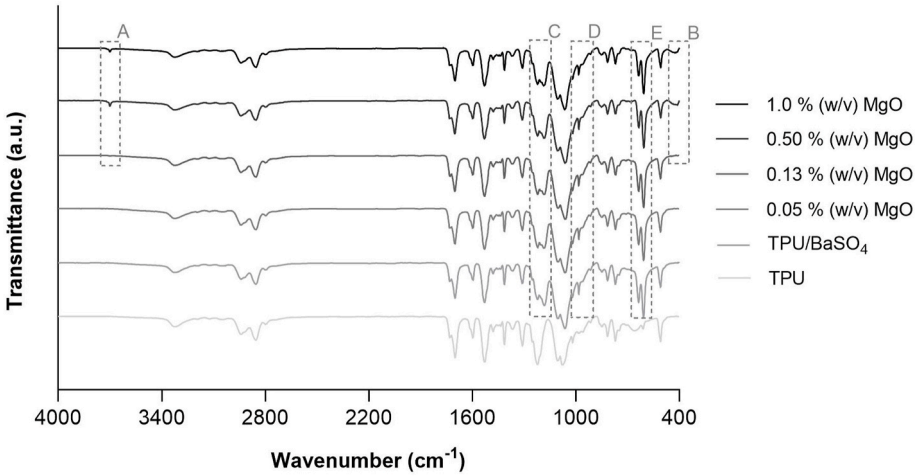

Fig. 4. – FTIR spectra of TPU and TPU/$BaSO_4$ films coated with different concentrations of MgO, highlighting key absorption peaks: A) The peak at 3700 cm^{-1} corresponding to the Hydroxyl (O–H) stretch; B) The peak at 420 cm^{-1} indicative of the Mg-O vibration; C) The peaks at 1225, 1182 cm^{-1} and D) 984 cm^{-1} characteristic of sulfate (SO_4^{2-}) stretch; E) The peaks at 636 and 610 cm^{-1} associated with the SO_4^{2-} bending vibrations. These spectra provide insights into the chemical bonding and interactions within the coatings at different MgO concentrations.

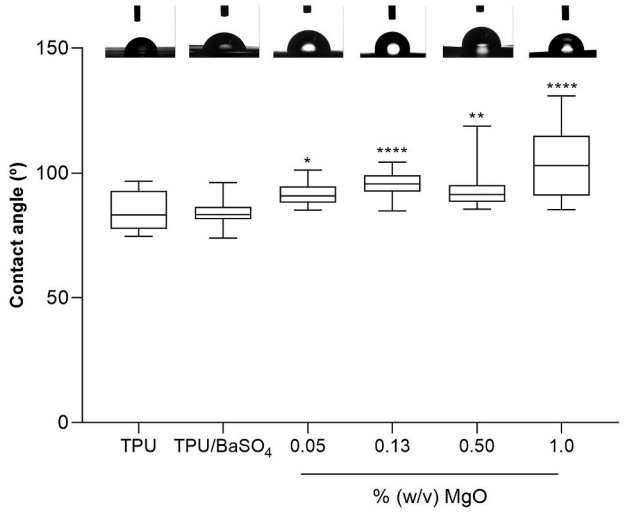

Fig. 5. – Water contact angle measurement using the captive bubble method on TPU/$BaSO_4$ films coated with different MgO concentrations, indicating the wettability of the surfaces. Statistically significant differences are as follows: * ($p < 0.05$), ** ($p < 0.001$), and **** ($p < 0.0001$), comparing each coated film to the TPU/$BaSO_4$ films as the control (One-way Anova analysis).

Table 1
– Results of Zeta potential measurements of TPU/$BaSO_4$ films coated with different MgO concentrations. Statistically significant differences compared to TPU/$BaSO_4$ films are indicated as *** ($p < 0.001$) and **** ($p < 0.0001$) (One-way Anova analysis).

Films surfaces	Zeta potential (mV)
TPU	−13.33 ± 2.76
TPU/$BaSO_4$	−12.42 ± 2.47
0.05 % (w/v) MgO	−16.71 ± 1. 56****
0.13 % (w/v) MgO	−16.17 ± 0.89****
0.50 % (w/v) MgO	−15.95 ± 2.64***
1.0 % (w/v) MgO	−20.35 ± 1.71****

3.2. Degradation studies

The chemical degradation of the different materials was evaluated according to ISO 10993–14:2001 standard using Tris–HCl as immersive media [38]. The degradation behavior was studied in terms of Mg release quantified through ICP and weight loss. Fig. 6 depicts the Mg concentration over immersion time. It was observed that an increase in MgO concentration coating on TPU/$BaSO_4$ films resulted in higher amounts of Mg released, as expected. Those samples coated with the lowest percentage of coating showed no release, with values close to 0, namely 0.31 ± 0.04 mg/L after day 1 and 0.42 ± 0.02 mg/L after 28 days. Samples with 0.13 % MgO coating released 0.97 ± 0.13 mg/L after day 1, maintaining values close to 1 mg/L at all time points up to day 28 with 1.17 ± 0.04 mg/L. Meanwhile, films with 0.50 % and 1.0 % MgO released 4.44 ± 0.54 mg/L and 10.0 ± 0.20 after day 1 and 4.66 ± 0.37 mg/L and 12.31 ± 0.87 mg/L after 28 days, respectively. All materials, independently of the MgO amount, showed a burst release after day 1, which remained constant for all 28 days.

In terms of weight loss, all samples maintained their weight throughout all time points, with no significant differences observed. This reinforces the stability of the materials and the coating over time.

The degradation tests were conducted with the primary objective to prove the stability of the coating over time since it is a crucial factor for the development of medical devices, namely the CVC. A release of MgO in large quantities could induce associated cytotoxicity effects. It is important to emphasize that the objective of this study was to ensure antibacterial performance while also guaranteeing biosafety. In this regard, as observed in the degradation studies, the coatings showed minimal release of MgO, particularly in the case materials with lower

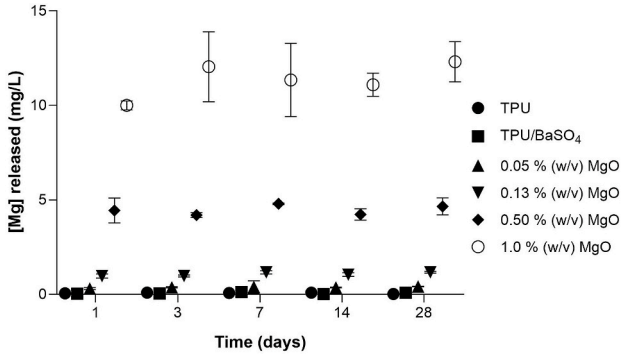

Fig. 6. – Amount of MgO released from TPU/$BaSO_4$ - MgO coated films over time, via inductively coupled plasma (ICP) analysis under degradation studies performed on materials for 28 days. The data highlights the stability of the MgO coating during the degradation process.

percentages of coating.

3.3. Antibacterial characterization

In previous studies reported in the literature on antimicrobial properties of MgO evaluation, different experimental techniques were used, different sizes and MgO nanoparticles concentrations, as well as varying initial seeding densities of bacteria. Consequently, the results from these studies are not directly comparable to each other and cannot be directly applied to the design of all antimicrobial materials formulations. For this purpose, the antibacterial properties of MgO used in this study were assessed by viable plate count method for MIC and MBC determination against *S. epidermidis*.

3.3.1. Minimum inhibitory concentration and minimum bactericidal concentration determination

CFUs quantification showed that the viability of bacteria was dependent on MgO concentration. The number of cultivable bacteria of *S. epidermidis* showed that concentrations of MgO above 0.5 mg/mL present a strong and significant reduction of bacterial growth, by approximately 99.98 % (4 logs) compared to bacteria control, and for higher concentrations, no bacterial growth was observed. MgO concentrations equal or above 1 mg/mL killed all the bacterial population during 24 h. The MIC and MBC for *S. epidermidis* were determined at 0.5 mg/mL and 1 mg/mL, respectively and the results are represented in Fig. S2 C (Supplementary Material).

The determination of the MIC for this oxide served as the baseline for defining the range of coating concentrations for the materials, starting from formulations with 0.05 % MgO (0.5 mg/mL).

3.3.2. Antibacterial activity of TPU/$BaSO_4$ – MgO coated films

The antibacterial performance of different TPU/$BaSO_4$ films coated with MgO on the growth of *S. epidermidis* is presented in Fig. 7 A, and B. The antibacterial activity was evaluated in terms of planktonic and sessile bacteria and the results are expressed as log_{10} (CFU/mL). For the 0.13 % concentration of MgO coating, a trend towards a decrease in the

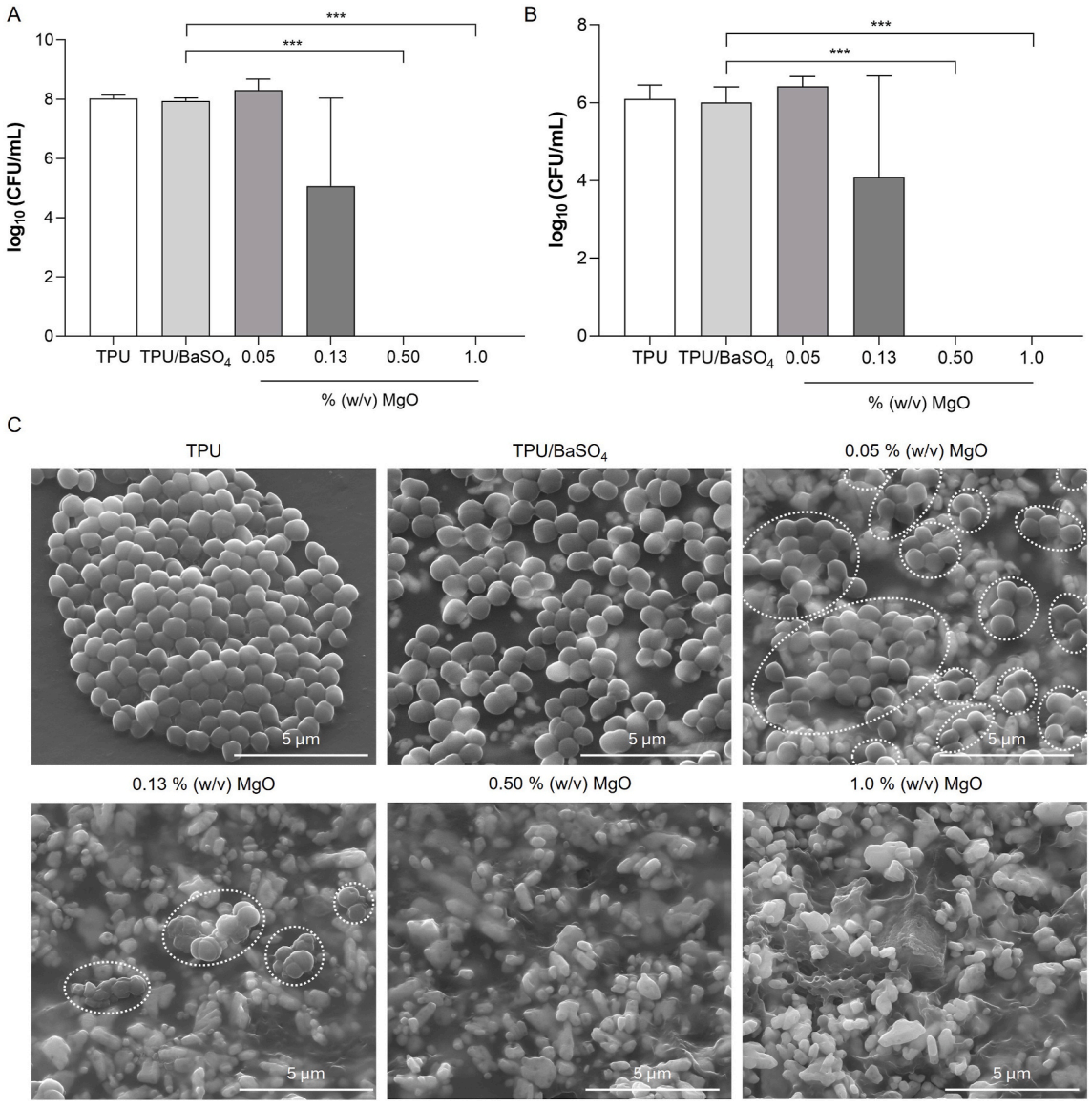

Fig. 7. Antibacterial activity of films coated with different concentrations of MgO after 24 h of incubation with *S. epidermidis*. A) Population of planktonic bacteria expressed in log_{10} (CFU/mL), and B) Population of sessile bacteria expressed in log_{10} (CFU/mL). C) SEM images of adherent *S. epidermidis* on the surfaces of TPU, TPU/$BaSO_4$, and TPU/$BaSO_4$ – MgO coated films. White circles were used to better visualize and highlight the presence of adhered bacteria to the surface (scale bar = 5 µm, magnification 20000x, HV 15 kV, SE mode). (***) Statistically significant differences compared to TPU/$BaSO_4$ films without MgO ($p < 0.001$; Kruskal-Wallis test).

number of viable bacteria is observed, with a 3-log reduction in planktonic bacteria and a 2-log reduction in adhered bacteria. For higher concentrations, bacterial growth inhibition becomes evident. Films coated with 0.50 and 1.0 % of MgO were able to completely inhibit planktonic growth (Fig. 7A) and adherent bacteria (Fig. 7B) after 24 h incubation, compared to the TPU/$BaSO_4$ films without MgO. On the contrary, there was no effect observed for 0.05 % MgO coated films in both assays.

The results from the bacterial adhesion assay were further supported by SEM analysis (Fig. 7C), which also displayed a similar reduction trend. Films coated with 0.50 % and 1.0 % MgO inhibited bacterial adhesion onto films' surfaces. Also, the SEM images show a significant decrease in the number of bacteria adhered to the surface for films with 0.13 % MgO. Furthermore, it is also clear that they lose their typical smooth shaped surface, which may have caused damage to the bacteria. SEM images also showed the typical spherical coccus morphology of *S. epidermidis* and bacteria clusters formation on surfaces without coating or with coatings but presenting the lowest MgO percentage.

The results obtained are in agreement with previous studies stating that MgO is capable of inhibiting gram-positive bacteria [51,52] and the antibacterial effect is dependent on the MgO concentration [40,53]. The antibacterial effect observed mainly in planktonic bacteria may be attributed to Mg ions release. As observed in previous degradation tests by ICP, increased loading in the coating led to higher Mg ions release into the medium after 24 h. In fact, the release of free ions is often referred as a mechanism for the toxicity of metal oxides [24]. MgO nanoparticles release Mg ions which can disrupt bacterial cell membrane and interfere with cellular processes, leading to cell death [30]. However, Nguyen et al. showed that the released Mg^{2+} ions from MgO was not the predominant mechanism since Mg^{2+} ions release and changes in pH were non-toxic and did not influence antibacterial activity of *S. epidermidis* [29].

A study by Leung et al. proposed that the primary mechanism of action of MgO involves the interaction between MgO nanoparticles and bacteria, resulting in cell membrane damage. It also suggested that the mechanism may be enhanced by combining with other phenomena like increased pH and Mg^{2+} release [28]. The direct interaction of bacteria membrane with the nanoparticle may cause cellular damage, the high surface area-to-volume ratio of MgO nanoparticles facilitates close contact with bacterial cells, promoting the efficient generation and diffusion of ROS into bacterial cells, enhancing their antimicrobial activity [54].

Other mechanism of action can be attributed to the antibacterial activity, MgO nanoparticles can generate reactive oxygen species (ROS) such as hydrogen peroxide (H_2O_2), hydroxyl ($OH^{\bullet}$) and superoxide radicals ($O_2^{\bullet-}$), that may induce oxidative stress in bacterial cells, damaging bacterial cell membranes, proteins, DNA, ultimately leading to bacterial cell death [32]. Several authors have attributed the antibacterial activity of MgO to the ROS production [25,30,55]. Krishnamoorthy et al. evaluated the antibacterial activity of MgO against gram-positive bacteria and proposed that the mechanism of the MgO antibacterial activity was due to the presence of defects or oxygen vacancies at the nanoparticles' surface, which caused formation of ROS and consequently led to the lipid peroxidation [32]. Sawai et al. investigated the bactericidal activity of MgO nanoparticles against both Gram-positive and Gram-negative bacteria. They suggested that the presence of active oxygen on the MgO surfaces, such as superoxide, is one of the key factors influencing their antibacterial activity [55].

Furthermore, MgO may disrupt bacterial adhesion and biofilm formation through physical and electrostatic interactions with bacterial cells. The negatively charged surface of MgO nanoparticles may repel negatively charged bacterial cells, thereby inhibiting their attachment to the coated surface.

Overall, these mechanisms of action of MgO coatings collectively contribute to their effective antibacterial properties. The hypothesis above may explain the good performance in terms of antibacterial behavior displayed by the coating samples on planktonic and adherent bacteria and may explain the differences observed between samples.

3.4. *In vitro cytotoxicity of TPU/$BaSO_4$ – MgO coated films*

Fig. 8 (A, B) shows the biocompatibility assessment results of the coatings using L929 mouse fibroblasts, with both direct and indirect contact assays performed according to ISO 10993-5 [43]. According to this ISO, a metabolic activity below 70 % indicates cytotoxic potential. After 24 h incubation, the metabolic activity of L929 cells in direct contact with our materials did not differ significantly from the negative control, suggesting that the materials are non-cytotoxic to L929 fibroblasts. For the indirect contact assay, where cell metabolic activity was measured after exposure to extracts of the coated films, all samples showed cell metabolic activity above 70 %, indicating no cytotoxicity. The exception was the 1 % MgO coated films, where a slight decrease in metabolic activity was observed. This reduction is probably due to the higher release of MgO at this concentration, as confirmed by ICP analysis. However, the metabolic activity remained above the limit for biocompatibility.

Fluorescence microscopy images from Live/dead cell viability assay (Fig. 8C) further support these findings. Most cells were viable and stained green, with a small number of dead cells visible in red, similar to the negative control L929.

The biocompatibility of the MgO coated films was evaluated by incubating viable fibroblasts in direct contact with the materials and by using extracts from the films to indirect contact. The direct contact test showed that the materials did not cause cytotoxicity, while indirect contact test ensured that any leachable species, did not induce cytotoxic effects. This biocompatible behavior is in accordance with findings reported by Krishnamoorthy et al., where no cytotoxicity towards human lung fibroblasts was observed [32].

3.5. *Hemocompatibility of TPU/$BaSO_4$ - MgO coated films*

The hemocompatibility of the developed films, both with or without MgO coating was also assessed by evaluating their hemolytic and antithrombogenicity potential (Fig. 9).

Studies depicted in Fig. 9A revealed that all surfaces exhibited hemolysis percentages below 5 %, thereby meeting the criteria outlined in ISO 10993-Biological evaluation of medical devices – Part 4: Selection of tests for interactions with blood, indicative of hemocompatible performance [56]. Considering the clotting time (Fig. 9B), the positive control (glass) exhibited complete clotting formation after 5 min incubation, while negative control (polystyrene, PS) showed clotting after 13 min. The control films without MgO coating (TPU and TPU/$BaSO_4$) exhibited an average clotting time of 15 and 13 min, respectively and films coated with MgO at different concentrations presented similar clotting formation times among themselves, closely resembling those of the controls and PS, approximately 12 min.

The potential to use these coated films for blood contact applications was also confirmed through *in vitro* hemocompatibility assays, which showed no hemolytic effects, and clotting time after contact with blood was similar to negative control. Since TPU and TPU with $BaSO_4$ are already used to produce CVCs, it is already known to be hemocompatible. The addition of a coating of MgO on the surface of TPU/$BaSO_4$ did not affect this property. These findings are in agreement with previously published data, indicating that MgO does not induce a hemolytic effect [57].

Regarding the antithrombogenic effect of the films, previous studies have suggested that Mg ions [34] and MgO [58] may influence blood clotting and consequently act as anticoagulants. Jankun et al. found that magnesium increases the clotting time in both plasma and whole blood in a concentration dependent manner [34]. Although our results did not directly demonstrate this effect on human plasma, it is important to note that the inclusion of MgO coating did not affect the clotting time of medical grade TPU and TPU/$BaSO_4$.

Films containing 0.50 % and 1.0 % MgO proved to be significantly

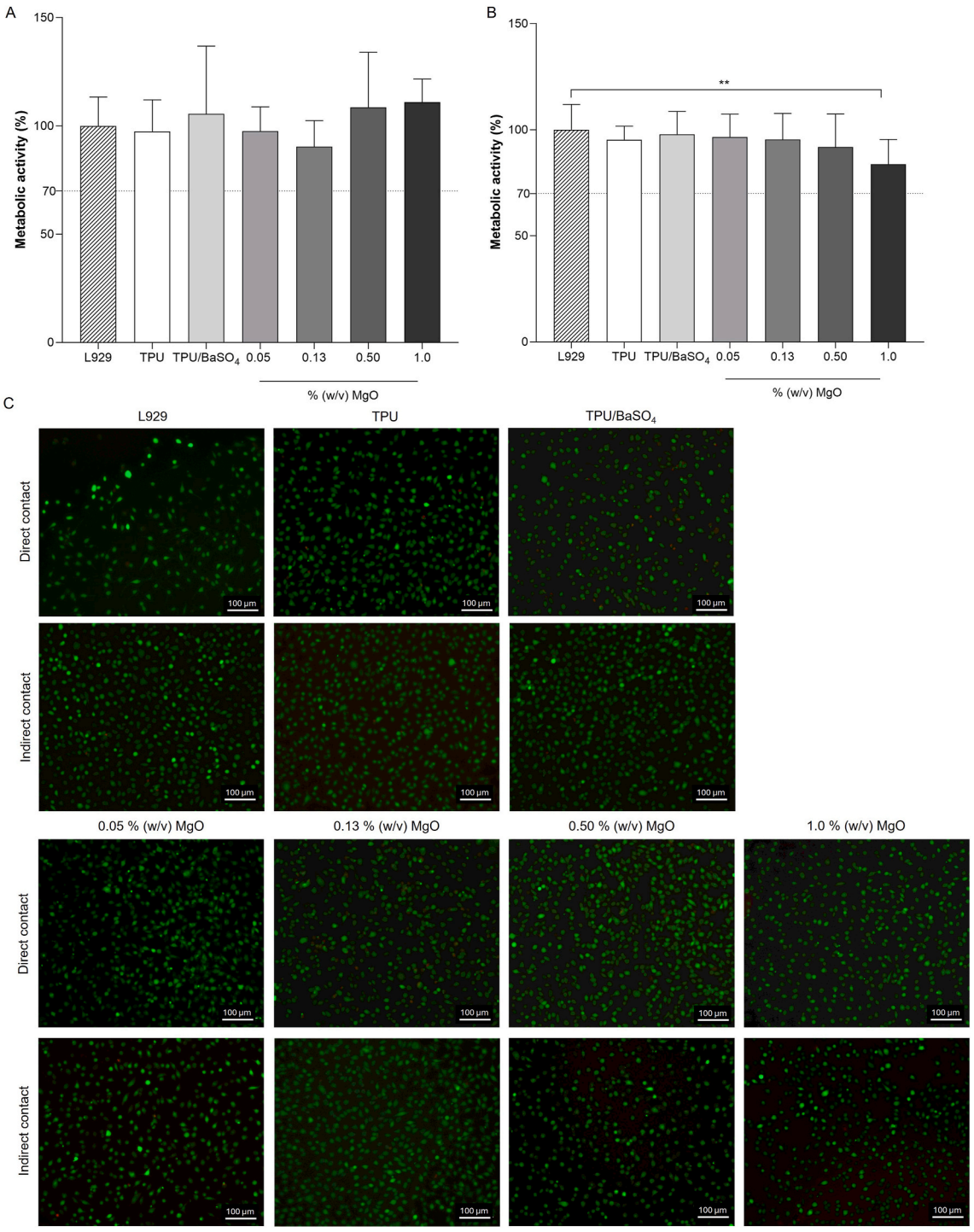

Fig. 8. – Evaluation of cytotoxicity of TPU/$BaSO_4$ – MgO coated films on L929 fibroblasts after 24 h of incubation. A) Metabolic activity of L929 fibroblasts assessed via direct contact using the resazurin assay, highlighting the impact of direct material-cell interactions on fibroblasts activity. B) Metabolic activity of L929 fibroblasts via indirect contact assay, evaluating the effects of leachable substances from material extracts on fibroblast metabolic activity. Results are expressed as the percentage of metabolic activity relative to the negative control. C) Representative fluorescence microscopy images from the Live/dead viability assay, where viable cells are stained green and dead cells are stained red (scale bar = 100 µm). (**) Statistically significant differences compared to the negative control ($p < 0.01$; Kruskal-Wallis test). (For interpretation of the references to colour in this figure legend, the reader is referred to the Web version of this article.)

antibacterial against a major pathogen associated with central venous catheter infections while also maintaining biocompatibility and hemocompatibility. These two coatings showed a significant release of Mg compared to the films without MgO, with the 1.0 % MgO coating, releasing twice the amount of magnesium when compared to 0.50 % MgO coating. Although the 1.0 % MgO coating formulation was not cytotoxic against fibroblasts, a decrease in metabolic activity was observed in indirect cell contact assays. Thus, the newly TPU/$BaSO_4$ – 0.50 % MgO coating appears to be the most advantageous, as it ensures the desired properties using a smaller amount of MgO, which may represent a significant reduction in economic terms. Given the expanding central venous catheter market, valued at over $2.6 billion in 2022 and growing at a compound annual growth rate (CAGR) of 6.4 % until 2032 with a projected valuation of $4.7 billion, the use of a reduced

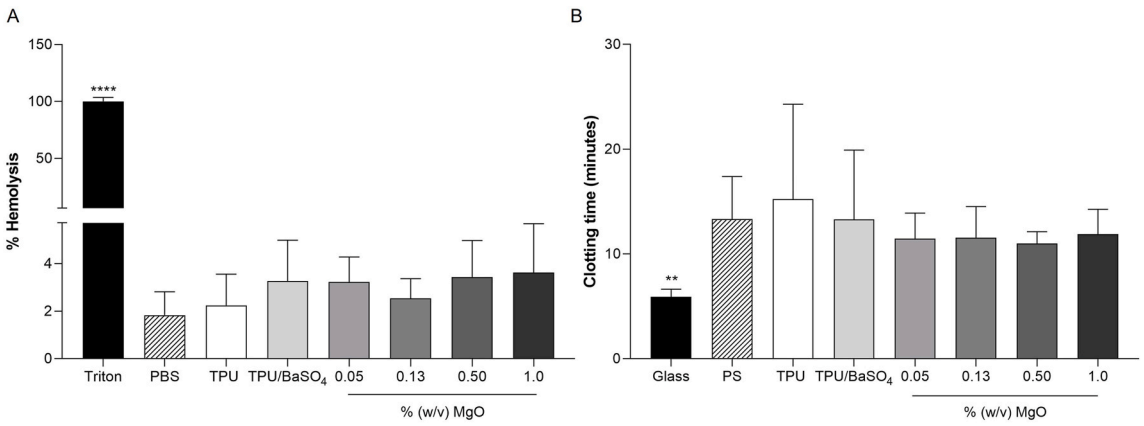

Fig. 9. – Hemocompatibility profile of TPU/$BaSO_4$ – MgO coated films. A) Hemolysis assay results, showing the percentage of hemolysis after incubation with red blood cells for 3h. PBS and 1 % Triton were used as negative and positive control, respectively. (****) Statistically significant differences compared to all other tested materials ($p < 0.05$; One-way Anova), (B) *In vitro* antithrombogenicity assay results, measuring the clotting potential of human recalcified plasma in contact with materials. **Statistically significant differences compared to the polystyrene (PS) ($p < 0.01$; One-way Anova).

amount of coating not only ensures significant economic savings but also enhances market viability [59].

4. Conclusions

This study successfully developed a novel coated surface for potential application in central venous catheters, addressing the critical need for infection prevention in medical devices. The incorporation of magnesium oxide (MgO) nanoparticles onto the TPU/$BaSO_4$ surface combined the inherent biocompatible and physicochemical properties of TPU while providing effective antibacterial functionality.

The study showed that MgO coatings, at concentrations of at least 0.50 % (w/v), completely eradicated both planktonic and adherent *Staphylococcus epidermidis*. Furthermore, comprehensive biocompatibility assessments demonstrated excellent biological safety. The coatings exhibited no significant cytotoxicity to fibroblasts showing also to be non-hemolytic and non-thrombogenic. Therefore, these coatings are suitable for blood-contact applications.

The straightforward and cost-effective coating method developed in this study maintains the intrinsic physical and chemical properties of TPU, supporting its scalability and practicality for industrial production. This versatile technique is not only suitable for central venous catheters but also adaptable for other medical devices, paving the way for broader applications of antimicrobial materials in healthcare. While this study represents a significant advancement in the development of antimicrobial coatings, future research should focus on investigating the mechanisms underlying the antibacterial activity of MgO. Understanding these mechanisms could further optimize the coating performance and expand its applicability in medical technology.

CRediT authorship contribution statement

Tatiana Padrão: Writing – review & editing, Writing – original draft, Validation, Methodology, Investigation, Formal analysis, Data curation, Conceptualization. **Fernando J. Monteiro:** Writing – review & editing, Validation, Supervision, Resources, Funding acquisition, Conceptualization. **Susana R. Sousa:** Writing – review & editing, Validation, Supervision, Resources, Funding acquisition, Conceptualization. **Juliana R. Dias:** Writing – review & editing, Validation, Supervision, Resources, Funding acquisition, Conceptualization.

Declaration of competing interest

The authors declare that they have no known competing financial interests or personal relationships that could have appeared to influence the work reported in this paper.

Acknowledgements

This work was financially supported by the Fundação para a Ciência e a Tecnologia (FCT) through the Strategic Projects granted to CDRSP: UIDB/04044/2020 (https://doi.org/10.54499/UIDB/04044/2020), UIDP/04044/2020 (https://doi.org/10.54499/UIDP/04044/2020), to the Associate Laboratory ARISE (LA/P/0112/2020) and PTCentroDiH project (03/C16-i03/2022-768); the grant awarded to Tatiana Padrão 10.54499/2020.09198.BD (https://doi.org/10.54499/2020.09198.BD) and the funding to Juliana Dias (10.54499/CEECINST/00060/2021/CP2902/CT0005). This study was also supported by "OP-SMARTherapy, 2022.04238.PTDC", "InnovaBIOMAS, 2022.10564.PTDC", INOV.AM – Inovação em Fabricação Aditiva, 02-C05-i01.01–2022, PC644865234-00000004 (WP14) and by European Union through PREDICTOS "PREDICTOS, 101079372". This study was also supported by i3s -Instituto de investigação e Inovação em Saúde da Universidade do Porto (POCI-01-0145-FEDER-007274), financed by FEDER – Fundo Europeu de Desenvolvimento Regional funds through the COMPETE 2020 and Portugal 2020. The authors would like to acknowledge to the i3S Scientific Platforms, members of the national infrastructure PPBI – Portuguese Platform of Bioimaging (PPBI-POCI-01-0145-FEDER-022122 and UIDB/04293/2020). Specially we acknowledge Ricardo Vidal from Biointerfaces and Nanotechnology platform for the assistance in FTIR, contact angle and zeta potential, as well as to Sofia Pacheco and Rui Fernandes from Histology and Electron Microscopy platform for TEM imaging. The authors also acknowledge Rui Rocha from CEMUP-Centro de Materiais da Universidade do Porto for his assistance in SEM analysis.

Appendix A. Supplementary data

Supplementary data to this article can be found online at https://doi.org/10.1016/j.ceramint.2025.01.376.

References

[1] H.A. Khan, F.K. Baig, R. Mehboob, Nosocomial infections: epidemiology, prevention, control and surveillance, Asian Pac. J. Trop. Biomed. 7 (2017) 478–482.
[2] A. Bowdle, L.S. Munoz-Price, Preventing Infection of Patients and Healthcare Workers Should Be the New Normal in the Era of Novel Coronavirus Epidemics, vol. 132, 2020, pp. 1292–1295.
[3] S.-L. Almeida, Health care–associated infections (HAIs), J. Emerg. Nurs. 41 (2020) 100.
[4] Z.K. Zander, M.L. Becker, Antimicrobial and Antifouling Strategies for Polymeric Medical Devices, ACS Publications, 2018.

[5] S.L. Percival, L. Suleman, C. Vuotto, G. Donelli, Healthcare-associated infections, medical devices and biofilms: risk, tolerance and control, J. Med. Microbiol. 64 (2015) 323–334.

[6] A. Zorgani, A. Abofayed, A. Glia, A. Albarbar, S. Hanish, Prevalence of device-associated nosocomial infections caused by gram-negative bacteria in a trauma intensive care unit in Libya, Oman Med. J. 30 (2015) 270.

[7] R.A. Weinstein, R.O. Darouiche, Device-associated infections: a macroproblem that starts with microadherence, Clin. Infect. Dis. 33 (2001) 1567–1572.

[8] H. Hanna, P. Bahna, R. Reitzel, T. Dvorak, G. Chaiban, R. Hachem, I. Raad, Comparative in vitro efficacies and antimicrobial durabilities of novel antimicrobial central venous catheters, Antimicrob. Agents Chemother. 50 (2006) 3283–3288.

[9] C. Casimero, T. Ruddock, C. Hegarty, R. Barber, A. Devine, J. Davis, Minimising blood stream infection: developing new materials for intravascular catheters, Medicines 7 (2020) 49.

[10] D.G. Maki, D.M. Kluger, C.J. Crnich, The risk of bloodstream infection in adults with different intravascular devices: a systematic review of 200 published prospective studies, in: Mayo Clinic Proceedings, Elsevier, 2006, pp. 1159–1171.

[11] I. Raad, H. Hanna, D. Maki, Intravascular catheter-related infections: advances in diagnosis, prevention, and management, Lancet Infect. Dis. 7 (2007) 645–657.

[12] R. Gahlot, C. Nigam, V. Kumar, G. Yadav, S. Anupurba, Catheter-related bloodstream infections, Int. J. Critical Illness Injury Sci. 4 (2014) 162–167.

[13] B. Böll, E. Schalk, D. Buchheidt, J. Hasenkamp, M. Kiehl, T.R. Kiderlen, M. Kochanek, M. Koldehoff, P. Kostrewa, A.Y. Claßen, Central venous catheter–related infections in hematology and oncology: 2020 updated guidelines on diagnosis, management, and prevention by the Infectious Diseases Working Party (AGIHO) of the German Society of Hematology and Medical Oncology (DGHO), Ann. Hematol. 100 (2021) 239–259.

[14] A. Shrivastava, S. Singh, P. Taank, K.B. Kaur, K. Pradip, V. Marwah, M. Sood, Incidence, risk factors, and microbiology of central venous catheterization-associated bloodstream infections at a surgical tertiary intensive care unit, J. Sci. Soc. 48 (2021) 28.

[15] R. Berardi, S. Rinaldi, D. Santini, B. Vincenzi, R. Giampieri, E. Maccaroni, F. Marcucci, M. Francoletti, A. Onofri, A. Lucarelli, Increased rates of local complication of central venous catheters in the targeted anticancer therapy era: a 2-year retrospective analysis, Support. Care Cancer 23 (2015) 1295–1302.

[16] J.-F. Timsit, Y. Dubois, C. Minet, A. Bonadona, M. Lugosi, C. Ara-Somohano, R. Hamidfar-Roy, C. Schwebel, New materials and devices for preventing catheter-related infections, Ann. Intensive Care 1 (2011) 1–9.

[17] W.V. Kern, Infections Associated with Intravascular Lines and Grafts, Infections Diseases, Fourth Edition, 2017.

[18] A.L. Casey, L.A. Mermel, P. Nightingale, T.S. Elliott, Antimicrobial central venous catheters in adults: a systematic review and meta-analysis, Lancet Infect. Dis. 8 (2008) 763–776.

[19] M. Gominet, F. Compain, C. Beloin, D. Lebeaux, Central venous catheters and biofilms: where do we stand in 2017? Apmis 125 (2017) 365–375.

[20] G. Gebreyohannes, A. Nyerere, C. Bii, D.B. Sbhatu, Challenges of intervention, treatment, and antibiotic resistance of biofilm-forming microorganisms, Heliyon 5 (2019) e02192.

[21] N.P. O'Grady, M. Alexander, L.A. Burns, E.P. Dellinger, J. Garland, S.O. Heard, P. A. Lipsett, H. Masur, L.A. Mermel, M.L. Pearson, Guidelines for the prevention of intravascular catheter-related infections, Clin. Infect. Dis. 52 (2011) e162–e193.

[22] K.N. Stevens, O. Crespo-Biel, E.E. van den Bosch, A.A. Dias, M.L. Knetsch, Y. B. Aldenhoff, F.H. van der Veen, J.G. Maessen, E.E. Stobberingh, L.H. Koole, The relationship between the antimicrobial effect of catheter coatings containing silver nanoparticles and the coagulation of contacting blood, Biomaterials 30 (2009) 3682–3690.

[23] A. Khoo, P. Oziemski, Chlorhexidine impregnated central venous catheter inducing an anaphylatic shock in the intensive care unit, Heart Lung Circ. 20 (2011) 669–670.

[24] S.M. Dizaj, F. Lotfipour, M. Barzegar-Jalali, M.H. Zarrintan, K. Adibkia, Antimicrobial activity of the metals and metal oxide nanoparticles, Mater. Sci. Eng. C 44 (2014) 278–284.

[25] J. Sawai, Quantitative evaluation of antibacterial activities of metallic oxide powders (ZnO, MgO and CaO) by conductimetric assay, J. Microbiol. Methods 54 (2003) 177–182.

[26] P. Makvandi, C.y. Wang, E.N. Zare, A. Borzacchiello, L.n. Niu, F.R. Tay, Metal-based nanomaterials in biomedical applications: antimicrobial activity and cytotoxicity aspects, Adv. Funct. Mater. 30 (2020) 1910021.

[27] M.J. Hajipour, K.M. Fromm, A.A. Ashkarran, D.J. de Aberasturi, I.R. de Larramendi, T. Rojo, V. Serpooshan, W.J. Parak, M. Mahmoudi, Antibacterial properties of nanoparticles, Trends Biotechnol. 30 (2012) 499–511.

[28] Y.H. Leung, A.M. Ng, X. Xu, Z. Shen, L.A. Gethings, M.T. Wong, C.M. Chan, M. Y. Guo, Y.H. Ng, A.B. Djurišić, Mechanisms of antibacterial activity of MgO: non-ROS mediated toxicity of MgO nanoparticles towards Escherichia coli, Small 10 (2014) 1171–1183.

[29] N.-Y.T. Nguyen, N. Grelling, C.L. Wetteland, R. Rosario, H. Liu, Antimicrobial activities and mechanisms of magnesium oxide nanoparticles (nMgO) against pathogenic bacteria, yeasts, and biofilms, Sci. Rep. 8 (2018) 16260.

[30] P. Bhattacharya, A. Dey, S. Neogi, An insight into the mechanism of antibacterial activity by magnesium oxide nanoparticles, J. Mater. Chem. B 9 (2021) 5329–5339.

[31] Z.-X. Tang, B.-F. Lv, MgO nanoparticles as antibacterial agent: preparation and activity, Braz. J. Chem. Eng. 31 (2014) 591–601.

[32] K. Krishnamoorthy, J.Y. Moon, H.B. Hyun, S.K. Cho, S.-J. Kim, Mechanistic investigation on the toxicity of MgO nanoparticles toward cancer cells, J. Mater. Chem. 22 (2012) 24610–24617.

[33] C.L. Wetteland, J. de Jesus Sanchez, C.A. Silken, N.-Y.T. Nguyen, O. Mahmood, H. Liu, Dissociation of magnesium oxide and magnesium hydroxide nanoparticles in physiologically relevant fluids, J. Nanoparticle Res. 20 (2018) 1–17.

[34] J. Jankun, E. Skrzypczak-Jankun, B. Lipinski, Experimental immunology Complex function of magnesium in blood clot formation and lysis, Cent. Eur. J. Immunol. 38 (2013) 149–153.

[35] E.G. Souza, K. Kruger, C.D. Nascimento, C. Aguzzoli, G. Hoff, A.C.B. Moraes, R. G. Lund, P.S. Nascente, C.E. Cuevas-Suárez, E. Piva, Development of lead-free radiation shielding material utilizing barium sulfate and magnesium oxide as fillers in addition cure liquid silicone rubber, Polymers 15 (2023) 4382.

[36] M. Martins, D. Wang, J. Ji, L. Feng, M. Barbosa, Albumin and fibrinogen adsorption on PU–PHEMA surfaces, Biomaterials 24 (2003) 2067–2076.

[37] I. Borges, P.C. Henriques, R.N. Gomes, A.M. Pinto, M. Pestana, F.D. Magalhaes, I. C. Goncalves, Exposure of smaller and oxidized graphene on polyurethane surface improves its antimicrobial performance, Nanomaterials 10 (2020) 349.

[38] ISO 10993-14:2001 Biological Evaluation of Medical Devices—Part 14: Identification and Quantification of Degradation Products from Ceramics, International Organization of Standardization, Geneva, 2001.

[39] M.A. Wikler, Methods for Dilution Antimicrobial Susceptibility Tests for Bacteria that Grow Aerobically: Approved Standard, vol. 26, Clsi (Nccls), 2006.

[40] T. Jin, Y. He, Antibacterial activities of magnesium oxide (MgO) nanoparticles against foodborne pathogens, J. Nanoparticle Res. 13 (2011) 6877–6885.

[41] K. Krishnamoorthy, G. Manivannan, S.J. Kim, K. Jeyasubramanian, M. Premanathan, Antibacterial activity of MgO nanoparticles based on lipid peroxidation by oxygen vacancy, J. Nanoparticle Res. 14 (2012) 1–10.

[42] ISO 22196, Measurement of Antibacterial Activity on Plastics and Other Non-porous Surfaces, International Organization for Standardization, Vernier Geneva, Switzerland, 2011, 2011.

[43] ISO 10993-5: 2009-Biological Evaluation of Medical Devices-Part 5: Tests for in Vitro Cytotoxicity, International Organization for Standardization, 2009.

[44] D. Moura, A.T. Pereira, H.P. Ferreira, C.C. Barrias, F.D. Magalhães, H. Bergmeister, I.C. Gonçalves, Poly (2-hydroxyethyl methacrylate) hydrogels containing graphene-based materials for blood-contacting applications: from soft inert to strong degradable material, Acta Biomater. 164 (2023) 253–268.

[45] A.M. Pinto, C. Gonçalves, D.M. Sousa, A.R. Ferreira, J.A. Moreira, I.C. Gonçalves, F. D. Magalhaes, Smaller particle size and higher oxidation improves biocompatibility of graphene-based materials, Carbon 99 (2016) 318–329.

[46] M. Zhang, B. Zhang, X. Li, Z. Yin, X. Guo, Synthesis and surface properties of submicron barium sulfate particles, Appl. Surf. Sci. 258 (2011) 24–29.

[47] C.M. Patel, M. Chakraborty, Z. Murthy, Study on the stability and microstructural properties of barium sulfate nanoparticles produced by nanomilling, Adv. Powder Technol. 25 (2014) 226–235.

[48] B. Choudhury, A. Choudhury, Microstructural, optical and magnetic properties study of nanocrystalline MgO, Mater. Res. Express 1 (2014) 025026.

[49] T. Zhao, H. Chen, J. Zheng, Q. Yu, Z. Wu, L. Yuan, Inhibition of protein adsorption and cell adhesion on PNIPAAm-grafted polyurethane surface: effect of graft molecular weight, Colloids Surf. B Biointerfaces 85 (2011) 26–31.

[50] H.H. Tuson, D.B. Weibel, Bacteria–surface interactions, Soft Matter 9 (2013) 4368–4380.

[51] N. Aničić, M. Vukomanović, T. Koklič, D. Suvorov, Fewer defects in the surface slows the hydrolysis rate, decreases the ROS generation potential, and improves the non-ROS antimicrobial activity of MgO, Small 14 (2018) 1800205.

[52] C.C. Coelho, T. Padrão, L. Costa, M.T. Pinto, P.C. Costa, V.F. Domingues, P. A. Quadros, F.J. Monteiro, S.R. Sousa, The antibacterial and angiogenic effect of magnesium oxide in a hydroxyapatite bone substitute, Sci. Rep. 10 (2020) 19098.

[53] I. Perelshtein, G. Applerot, N. Perkas, J. Grinblat, E. Hulla, E. Wehrschuetz-Sigl, A. Hasmann, G. Guebitz, A. Gedanken, Ultrasound radiation as a "throwing stones" technique for the production of antibacterial nanocomposite textiles, ACS Appl. Mater. Interfaces 2 (2010) 1999–2004.

[54] G.C. Cotton, N.R. Lagesse, L.S. Parke, C.J. Meledandri, Antibacterial Nanoparticles, 2019.

[55] J. Sawai, H. Kojima, H. Igarashi, A. Hashimoto, S. Shoji, T. Sawaki, A. Hakoda, E. Kawada, T. Kokugan, M. Shimizu, Antibacterial characteristics of magnesium oxide powder, World J. Microbiol. Biotechnol. 16 (2000) 187–194.

[56] ISO 10993-4:2006 Biological Evaluation of Medical Devices- Part 4: Selection of Tests for Interaction with Blood, International Organization for Standardization, Geneva, Switzerland, 2006.

[57] H. Derakhshankhah, H. Nekounam, Z. Izadi, Z. Allahyari, M. Samari, H. Samadian, Fabrication of electroactive nanocomposite based on carbon nanofibers/magnesium oxide nanoparticles for bone tissue engineering, J. Drug Deliv. Sci. Technol. 89 (2023) 105082.

[58] M.M. Venkatappa, C. Udagani, S.M. Hanumegowda, S.N. Pramod, S. Venkataramaiah, R. Rangappa, R. Achur, A. Alataway, A.Z. Dewidar, M. Al-Yafrsi, Effect of Biofunctional Green synthesized MgO-nanoparticles on oxidative-stress-induced tissue damage and thrombosis, Molecules 27 (2022) 5162.

[59] A.M. Research, Central Venous Catheter Market Size, Share, Competitive Landscape and Trend Analysis Report by Product Type, by Property, by Design, by End-User : Global Opportunity Analysis and Industry Forecast, 2023-2032, Central Venous Catheter Market Global Opportunity Analysis and Industry Forecast, 2023-2032, 2023, p. 250.